31st Annual International Conference of the IEEE EMBS
Minneapolis, Minnesota, USA, September 2-6, 2009

In Silico Estimates of Cell Electroporation by Electrical Incapacitation Waveforms

T. R. Gowrishankar*, A. T. Esser*, K. C. Smith*,†, S. K. Burns*,‡, and J. C. Weaver*,§

***Abstract*— We use a system model of a cell and approximate magnitudes of electrical incapacitation (EI) device waveforms to estimate conditions that lead to responses with or without electroporation (EP) of cell membranes near electrodes. Single pulse waveforms of Taser X26 and Aegis MK63 devices were measured using a resistive load. For the present estimates the digitized waveforms were scaled in magnitude according to the inverse square radial distance from two tissue-penetrating electrodes, approximated as hemispheres. The corresponding tissue level electric fields were then used as inputs to the cell system model. A dynamic pore model for membrane electroporation (EP) was assigned to many different sites on the cell plasma membrane (PM). EI devices generate sufficiently large transmembrane voltage, $\mathrm{U_m(t)}$, such that pores were created, evolving into a heterogeneous and time-dependent pore population. These approximate responses suggest that both waveforms can cause PM EP. Peripheral nerve damage by EP is a candidate side effect. More extensive EP is expected from the Taser X26 than the Aegis MK63, mainly due to the approximately eight-fold difference in the peak magnitudes. In silico examination of EI waveforms by multiscale modeling is warranted, and can involve whole body, tissue and cell level models that now exist and are rapidly being improved.**

I. INTRODUCTION

Electrical incapacitation (EI) is a fundamentally attractive intervention option. This class of devices has the desirable prospect of providing rapid temporary human incapacitation, with more control and fewer side effects than mechanical methods (guns and clubs). Most chemical agents are not allowed by international treaty [3] and are difficult to control. Human nervous system cells and skeletal muscle cells are excitable, controllable by small changes in the transmembrane voltage, U_m. Disruption of normal neuro-muscular control can result from the application of high voltage electric field pulses, with peripheral nerves a candidate for involvement in EI initiation [4]. Although electrical incapacitation devices may not be medical devices, they can have medical consequences. Further, in most cases an incapacitating electrical exposure is involuntary to the subject.

There have been reports of acute side effects, mainly cardiac. Less attention seems to have been given to the possibility of non-lethal long term effects, such as complex delayed physical injury and psychological problems in electrical shock patients [5], [6]. Electroporation (EP) is an established non-thermal contributor to electrical injury [7]. In addition to Joule tissue heating, large skeletal muscle and nerve cells can be injured by biochemical imbalances through molecular and ionic loss or uptake by cell EP. For example, twelve electric field pulses of $4\,\mathrm{ms}$ duration and magnitudes of only 75 and $150\,\mathrm{V/cm}$ can cause peripheral nerve damage [8]. With this in mind here we consider the question of whether EI waveforms might cause EP of cells near electrodes. In this initial exploratory study we consider a model of a typical isolated mammalian cell ($r_\mathrm{cell} = 10\,\mu\mathrm{m}$; Fig. 1a) which is exposed to electric field waveforms that are estimated to occur at different distances from idealized representations (hemispheres) of electrodes that penetrate slightly into tissue.

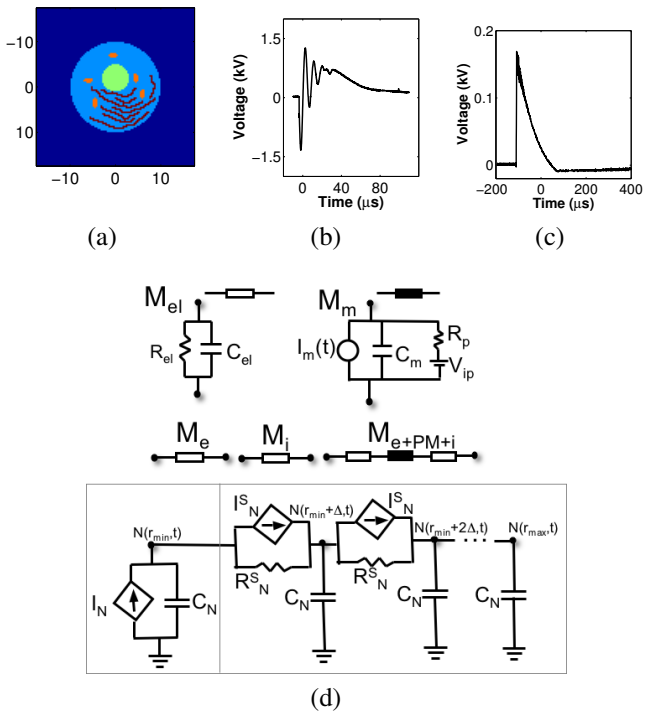

Fig. 1. **(a)** Cell system model 2D geometry with dimensions shown in μm (see II. C). **(b)** Measured waveforms of a Taser X26 and **(c)** of an Aegis MK63 interpolated for a 400 Ω load from different load measurements. **(d)** Local circuit models for electrolyte (M_{el}) and membrane (M_m) are assembled in different configurations to represent electrolytes and electrolyte/membrane interfaces (only PM model is shown here). Equivalent circuit representation of the dynamic EP model (bottom panel) is distinguished from the asymptotic EP model (left box in the bottom panel). The circuit models and their configurations are described in detail in [1], [2].

* Harvard-MIT Division of Health Sciences and Technology, Massachusetts Institute of Technology, Cambridge, MA 02139, USA
† Department of Electrical Engineering and Computer Science, Massachusetts Institute of Technology, Cambridge, MA 02139, USA.
‡ Burns Consulting, Durham, NH 03824, USA.
§ Corresponding author: jcw@mit.edu
Supported by NIH Grant RO1-GM63857 and Aegis Industries, Inc.

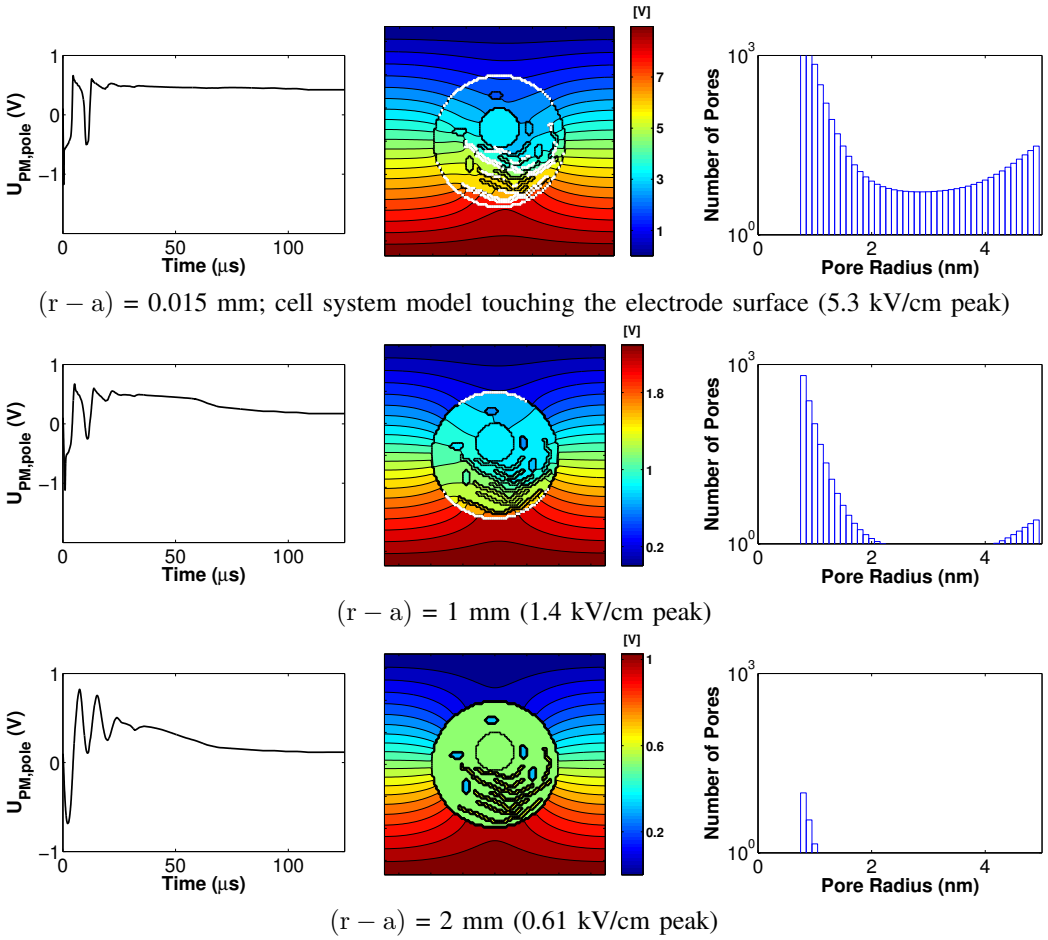

Fig. 2. Response of the cell model to a Taser X26 waveform. Left: Transmembrane voltage at the anodic (bottom) pole. Middle: Equipotential lines and electroporated sites (shown in white where number of local pores $\geq$ 10) at t=39 μs. Right: PM Pore histograms (total number of pores over the entire PM centered for each pore radius) with a bin width of 0.1 nm at t=39 μs. The three rows of panels show the response at different distances from the edge of the electrode. At distances of 0.015 mm and 1 mm from the electrode, some pores have evolved to more than 4 nm in radius. At 0.015 mm from the electrode certain organelle membranes are also electroporated, signifying a large intracellular electric field.

II. METHODS

A. Waveform measurements.

Two electrical incapacitation devices (Taser X26 and Aegis MK63) were measured for several resistive loads and interpolated to give peak loaded waveform voltages, $V_{\rm app}(t)$, for a $400\,\Omega$ load (Burns Consulting, Durham, NH). The waveforms (Figs. 1b and 1c) were then digitized to provide voltages, $V_{\rm app}(t)$, that in the present estimates were applied to a pair of hemispherical electrodes.

B. Hemispherical model for tissue penetrating electrodes.

We used a simple electrode geometry to estimate the electric field near typical fixed protruding electrodes ("drive electrodes"). Specifically, we assumed metallic (high conductivity) hemispheres of radius $a = 1\,\mathrm{mm}$. We used the simplifying hemispherical approximation for the spreading resistance of an electrode in which the electrode separation is relatively unimportant [9]. The total resistance associated with heterogeneous fields concentrated near each electrode is $R_{1/2} \approx 1/[2\pi\sigma_{tiss}a]$, and with $\sigma_{\rm tiss}$ = 0.8 $S\,m^{-1}$, the total (load) resistance is $R \approx 1/\pi\sigma_{tiss}a = 400\,\Omega$. We use the quasi-electrostatic approximation with the waveform voltage, $V(t)$, to estimate the time dependent electric field at a radial distance, r, from the center of either electrode, $E(r,t) \approx [V(t)/2\pi\sigma_{tiss}R]/r^2$.

C. Cell system model construction and numerical solution.

The cell system model (Fig. 1a) includes the PM (10 μm radius), nuclear double membrane, the irregular shaped endoplasmic reticulum (ER) and five mitochondria (approximated with 1 $\mu m\times$ 2 μm cross sectional area), each with an outer and an inner membrane, separated by 15 nm of intermembrane space. The cell system model with the surrounding medium is represented by a Cartesian transport lattice. Adjacent nodes of the lattice are connected by electrical equivalent models (Fig. 1d) that represent either a conducting medium or a membrane. The PM and the outer mitochondrial membrane are represented by the dynamic EP model while the nuclear membrane, ER membrane and inner mitochondrial membrane are represented by the asymptotic EP model [10]. The details of the models and their circuit representations are described in [1], [2]. The equivalent

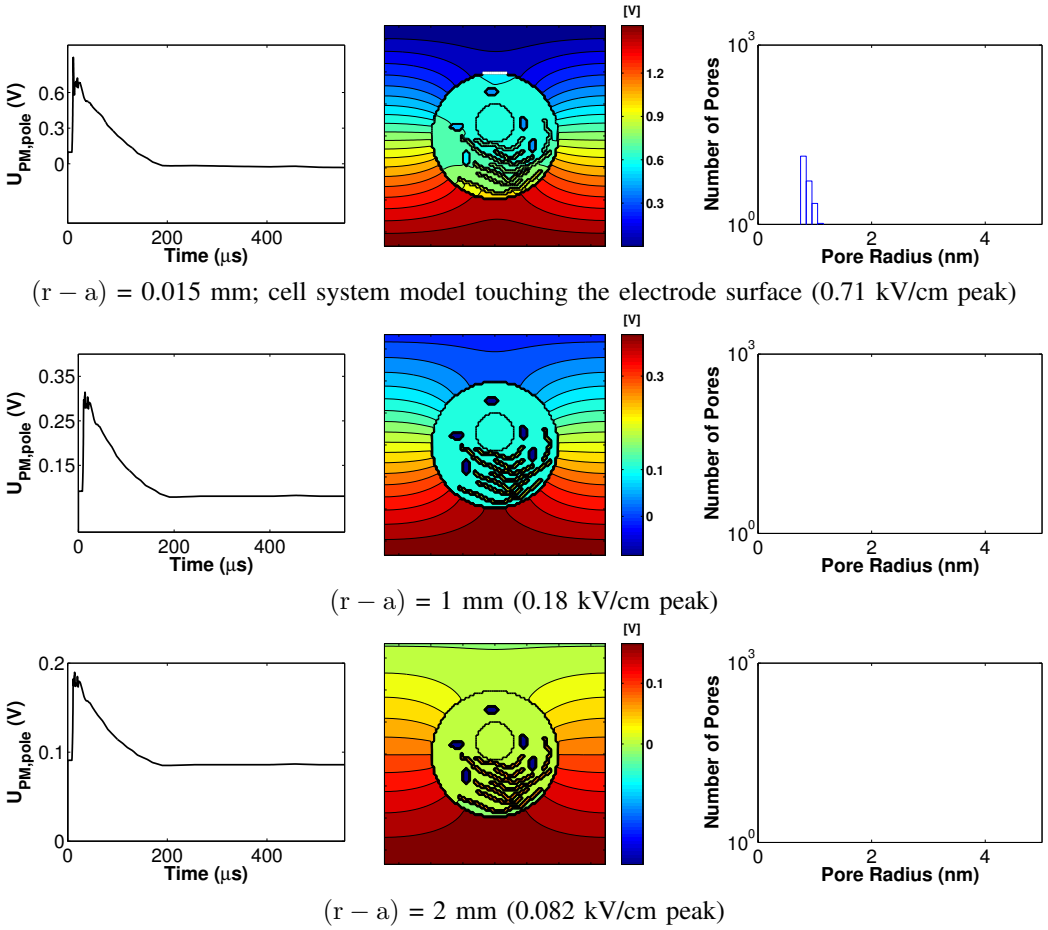

Fig. 3. Response of the cell model to an Aegis MK63 waveform. Left: Transmembrane voltage at the anodic pole. Middle: Equipotential lines and electroporated sites (shown in white where number of local pores $\geq$ 10) at t=39 μs. Right: PM Pore histograms (total number of pores over the entire PM centered at each pore radius) with a bin width of 0.1 nm at t=39 μs. The three rows of panels show the response at different distances from the edge of the electrode. At distances of 1 mm and 2 mm from the electrode the local field is not large enough to cause any PM EP.

system model results in a very large electrical circuit that was solved by Berkeley SPICE3f5.

For estimates of expected cell responses we chose radial distances of $r = 0.015$, 1 and 2 mm into the tissue from the edge of a hemispherical electrode. $\bar{E}(r,t) = E_{app}(t)$, the spatially averaged magnitude centered at r, is treated as uniform across the cell system model. The "height" of the system model, $L_{\rm sys} = 30\,\mu m$, corresponding to 101 nodes each separated by $0.3\,\mu$m.

III. RESULTS AND DISCUSSION

Figs. 2 and 3 show the model's response to the two different waveforms at three sites near an electrode. Black lines are equipotentials. Colored regions, ranging from dark blue (cathodic) to dark red (anodic), represent voltage ranges shown in the colorbars (larger for the X26). $E_{\rm app}(t)$ would be spatially uniform if the cell were replaced by aqueous extracellular medium.

For small fields, the response field within the system model is non-uniform, tending to go around the cell. Relatively small intracellular fields occur by displacement currents, and no EP occurs (no white regions). This behavior is observed at 2 mm for the X26 waveform (Fig. 2c), and at both 1 and 2 mm distances for the MK63 waveform (Fig. 3b and 3c). In these cases, the response field, $E_{\rm res}(t)$, that occurs with the cell present has the $V_{\rm app}(t)$ time dependence in the extracellular medium, and the extracellular field, $E_{\rm ext}(t)$, is non-uniform because of the cell being confined to a small volume. The intracellular field, $E_{\rm int}(t)$, is also non-uniform, due to the PM and the several organelles. The time dependence of both $E_{\rm int}(t)$, and $U_{\rm m}(t)$ at the PM and organelle membranes is different from $E_{\rm app}(t)$ because of spatially distributed charging of membranes and associated distributed displacement current densities for small fields.

At larger fields EP occurs (white regions), the response is further complicated by the time dependent pore creation which rapidly produces pore populations with a distribution of pore sizes. The rapidly changing pore distributions are based on $n(r,t)$ that varies over the plasma membrane (PM). Here $n(r,t)\Delta r$ is the total number of pores with radii between r and $r + \Delta r$, displayed as pore histograms with $\Delta r = 0.1$ nm in Figs. 2 and 3.

Yet another complication that has been addressed is the consequence of spatially distributed but different pore distri-

butions, which generate rapidly increasing local membrane conductance values that are different across the membrane. An immediate consequence is the significant change in ionic current density outside and mostly inside the cell, which in turn alters U_{m}, and that then alters the rate of local membrane conductance change. Our solutions are approximate, but take these complex interplays into account to generate estimates of EP pore histograms and conductance changes over the PM and organelle membranes for the measured waveforms.

Here we retain the traditional focus on PM EP, which is believed to be involved in non-thermal necrotic cell death by an elevated PM permeability due to the pores [7]. This degree of complexity leads to emergent behavior of EP within a multi-membrane system, and is far more complicated than the response of a traditional spherical PM to an electroporating pulse.

This is a step towards more realistic modeling of cells, which are multicompartment systems in which numerous organelles (some with interconnected interiors) are bathed in the cytoplasm and surrounded by the PM. The EP response of organelles seen at 1 mm from the X26 electrode is similar to the supra-EP response (pulses shorter than $1\,\mu$s that create pores with minimal expansion) [2], [11].

The peak values of the two waveforms for a load of $400\,\Omega$ are approximately $1,300\,\mathrm{V}$ for the X26 and $170\,\mathrm{V}$ for the MK63, an almost eight-fold difference. In general our models show that it is the peak waveform magnitude and duration, not the average voltage, that is important to EP. Why? Because the most widely accepted theoretical model for pore creation involves a Boltzmann factor with an argument that contains U_{m}^2, so pore creation is a strongly non-linear function of U_{m} [1], [2], [11]–[14]. This means that once a certain range of transmembrane voltages is reached, pore creation explodes, with the creation rate depending also on the rate at which U_{m} rises.

The most extensive EP occurs in Fig. 2 (top row). Inspection of the histogram shows that there are approximately 1,000 pores with $\sim$1 nm radius, and that adding up the pores in the bins with pore radius of at least 4 nm yields about 100 pores in this larger size range. Small ions can pass through the $\sim$1 nm pores, and significantly larger (e.g. $>$ 10 kDa) macromolecules can pass through the larger pores. This is consistent with the hypothesis that EP can cause cell death by non-thermal loss of essential molecules.

In summary, these estimates are based on simple idealized tissue-penetrating electrodes that allow approximate values of the tissue electric field near electrodes where the field is large because of current density concentration. The main point is that the irregular shaped measured EI waveforms are expected to cause PM EP in representative cell sizes. The results should be regarded as initial demonstrations that suggest more advanced models should be used in a similar fashion to estimate the conditions for non-thermal EP damage to peripheral nerves at various distances from EI-initiating electrodes. This can best be carried out by combing space-filling cell models with full or partial anatomically correct body models [15], [16], in which the electrode pairs are positioned at different locations, actual EI waveforms are applied to realistic models of electrodes, and the resulting fields within the body then be used as input to both individual cell [2], [14] and multi cell models [1], [11]. Estimates of loss of essential biochemicals from cells through heterogeneous, changing pore populations should provide important insight into the vulnerability of peripheral nerves to damage.

Some EI side effects are generally expected, but it is important to quantify them, and to carry out a research process in which efficacy of incapacitation is maximized while side effects are minimized.

REFERENCES

[1] A. T. Esser, K. C. Smith, T. R. Gowrishankar, and J. C. Weaver, "Towards solid tumor treatment by irreversible electroporation: Intrinsic redistribution of fields and currents in tissue," *Tech. Cancer Res. Treat.*, vol. 6, pp. 261–273, 2007.

[2] T. R. Gowrishankar, A. T. Esser, Z. Vasilkoski, K. C. Smith, and J. C. Weaver, "Microdosimetry for conventional and supra-electroporation in cells with organelles," *Biochem. Biophys. Res. Commun.*, vol. 341, pp. 1266–1276, 2006.

[3] I. R. Kenyon, K. Gutschmidt, and O. Cosivi, "Legal aspects and international asistance related to the deliberate use of chemicals to cause harm," *Toxicology*, vol. 214, pp. 249—255, 2005.

[4] F. Despa, S. Basati, Z.-D. Zhang, J. D'Andrea, J. P. Reilly, E. N. Bodnar, and R. C. Lee, "Electromuscular incapcitation results from stimulation of spinal reflexes (in press)," *Bioelectromagnetics*, 2009.

[5] N. H. Pliskin, A. N. Ammar, J. W. Fink, S. K. Hill, A. C. Malina, A. Ramati, K. M. Kelly, and R. C. Lee, "Neuropsychological changes following electrical injury," *J. Int. Neuropsychol. Soc.*, vol. 12, pp. 17–23, 2006.

[6] A. H. Wicklund, A. Ammar, J. C. Weitlauf, R. L. Heilbronner, J. Fink, R. C. Lee, K. Kelley, and N. H. Pliskin, "MMPI-2 patterns in electrical injury: A controlled investigation," *Clin. Neuropsychol.*, vol. 22, pp. 98–111, 2008.

[7] R. C. Lee, D. Zhang, and J. Hannig, "Biophysical injury mechanisms in electrical shock trauma," *Ann. Rev. Biomedical. Eng.*, vol. 2, pp. 477–509, 2000.

[8] G. S. Abramov, M. Bier, M. Capelli-Schellpfeffer, and R. C. Lee, "Alteration in sensory nerve function following electrical shock," *Burns*, vol. 22, pp. 602–606, 1996.

[9] J. Newman, "Resistance for flow of current to a disk," *J. Electrochem. Soc.*, vol. 113, pp. 501–502, 1966.

[10] J. C. Neu and W. Krassowska, "Asymptotic model of electroporation," *Phys. Rev. E*, vol. 59, pp. 3471–3482, 1999.

[11] T. R. Gowrishankar and J. C. Weaver, "Electrical behavior and pore accumulation in a multicellular model for conventional and supra-electroporation," *Biochem. Biophys. Res. Commun.*, vol. 349, pp. 643–653, 2006.

[12] I. G. Abidor, V. B. Arakelyan, L. V. Chernomordik, Y. A. Chizmadzhev, V. F. Pastushenko, and M. R. Tarasevich, "Electric breakdown of bilayer membranes: I. The main experimental facts and their qualitative discussion," *Bioelectrochem. Bioenerget.*, vol. 6, pp. 37–52, 1979.

[13] Z. Vasilkoski, A. T. Esser, T. R. Gowrishankar, and J. C. Weaver, "Membrane electroporation: The absolute rate equation and nanosecond timescale pore creation," *Phys. Rev. E*, vol. 74, p. 021904, 2006.

[14] D. A. Stewart, T. R. Gowrishankar, and J. C. Weaver, "Transport lattice approach to describing cell electroporation: use of a local asymptotic model," *IEEE Transactions on Plasma Science*, vol. 32, pp. 1696–1708, 2004.

[15] A. Christ, W. Kainz, E. Hahn, K. Honegger, J. Shen, W. Rascher, R. Janka, W. Bautz, B. Kiefer, P. Schmitt, H.-P. Hollenbach, J. Chen, A. Kam, E. Neufeld, M. Oberle, and N. Kuster, "The "Virtual Family" Project - Development of anatomical whole-body models of two adults and two children," in *Proceedings of the 23rd Annual Review of Progress in Applied Computational Electromagnetics (ACES) 2007*, Verona, Italy, 2007, session 16: Modeling of Biomedical Problems - 1 (March 21).

[16] S. Benkler, N. Chavannes, and N. Kuster, "Mastering conformal meshing for complex CAD-based C-FDTD simulations," *IEEE Antennas and Propagation Mag.*, vol. 50, pp. 45–56, 2008.